Monolayers and self-assembled bilayers on ITO for use in solar cells

Kardula, Jane

DOI:
10.33612/diss.1082120674

5

SYNTHESIS OF DASA SWITCHES FOR BILAYERS ON ITO

Abstract: *This chapter shows the synthesis of a second generations* ***DASAs*** *using 1,4-dimethylbarbituric acid and Meldrum acid as acceptors and TEG-ylated indoline as the donor part. Furthermore, we recorded their UV-Vis spectra and calculated the HOMO-LUMO gap of the target molecules.*

I would like to thank Tyl Wiglema for recording the UV-Vis spectras, Dr. Saurabh Soni and Natalia Paz Neme for the calculations of the HOMO-LUMO gap and transmission calculations. Rachael O. Hannah for the discussion about the synthesis of the DASAs.

5.1. INTRODUCTION

There are several types of organic photochroms that have been synthesized, including azobenzenes, stilbenes, spiropyrans, diarylethenes, hemithioindigo photoswitches, and acylhydrazone.[1–6] All of these switches shift their absorption maximum (λ_{max}) by undergoing cis-trans double-bond photoisomerization or light activated ring closing/opening.

Another class of switches that undergo light activated ring closing are the **D**onor-**A**cceptor **S**tenhouse **A**dducts (**DASAs**). The process of ring opening is thermally reversible. DASAs are a push-pull system where the acceptors are typically diketones or triketones, while the donor is amine-based.[7–11] The first generation of DASA switches use non-aromatic secondary amines that create zwitterionic systems when exposed to light. To avoid this, the second generation of DASA switches was developed using cyclic secondary amines. Researchers have also been working on developing new acceptors to replace Meldrum's acid and 1,3-dimethylbarbituric acid in order to shift the λ_{max} towards the near infrared region (NIR). DASA switches have an advantage over other switches such as spiropyrans and azobenzenes, which only absorb at 400 nm or less, because DASA switches shift the λ_{max} further towards the NIR.[12–15]

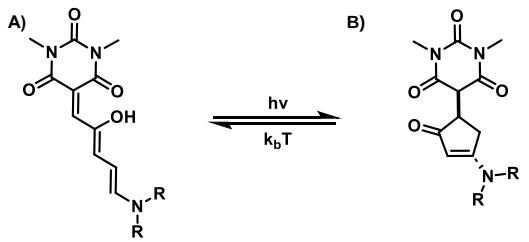

Scheme 5.1 DASA with N,N-dimethylbarbituric acid as an acceptor. **A)** Open form of DASA. **B)** Closed form of DASA.

The open form (**Scheme 5.1 A)**) of the compound has an extended π conjugated system from the donor and the triene, while the closed ring form (**Scheme 5.1 B)**) is formed through a E - Z isomerization followed by thermal 4π electrocyclization.[10–12] This closed ring form breaks the π conjugation, leading from a colored to a colorless solution also known as negative photochromism. Negative photochromism has the advantage of absorbing in the deeper layers of a solution, rather than just on the surface, which is the case with normal photochromism.[16] DASAs, with this negative photochromism property are an excellent option for solid-state orthogonal switching. To achieve orthogonal switching, it is necessary to use two different DASAs, one from the second generation and one from the third generation so the λ_{max} of both the switches do not overlap. This allows for selective switching of one of the DASAs based on the λ_{max}, resulting in four different states in the system. These states can be coded in such a way that the colored states are represented as 1 and the colorless state are represented as 0. Then we have 4 different possible states: (1,1) for both colored DASAs, (1,0) and (0,1) for one of the DASAs being colored and the other one colorless, and (0,0) for both colorless DASAs, allowing us to fabricate a device that can store information.

Self-assembled monolayers are frequently used to modify metal surfaces, with Au^{TS}

being one of the most commonly used metals. Studies by Kumar *et al.* have shown that spiropyran switches can be incorporated into mixed monolayers of thiols to alter the conductivity of the monolayer based on the state of the switch. While pristine monolayers of the spiropyran had significantly lower switching ratios, mixed monolayers were found to significantly improve performance due to optimized packing at the electrode interface.[17,18] To address the issues of oxidation and lower air stability associated with sulfides, Qui *et al.* employed a different approach.[19] The authors created bilayers on gold using PTEG-1 as the bottom monolayer and TEG-spiropyrans as the top monolayer, avoiding the use of sulfides. Utilizing TEG to form the bilayers, the authors demonstrated that glycol ethers are a suitable option for interdigitated bilayers. The success of the PTEG-1 bilayers inspired us to synthesize TEG-ylated DASAs for use in similar bilayers.

We have successfully synthesized TEG-ylated second generation DASAs using TEG-indoline as the donor and Meldrum's acid, 1,3-dimethylbarbituric acid as the acceptors. We also studied the impact of the TEG chain on the absorption by comparing Meldrum's acid using TEG-indole 6 and the methoxyindole Meldrum's acid DASA. Finally, Density Functional Theory (DFT) calculation[20,21] were performed using the Amsterdam Modeling Suite (AMS)[22] software with GGA-PBE[23] exchange-correlation functional and D3 as dispersion and TZP,[24,25] large frozen core and numerical accuracy using Becke 3 (good)[26] to calculations of the open and closed form DASA 5.

5.2. RESULTS & DISCUSSION

We began the synthesis of our target molecules by synthesizing the acceptors for the DASA switches. First, we used 1,3-dimethylpyrimidine-2,4,6(1H,3H,5H)-trione (1,3-dimethylbarbituric acid) and reacted it with furan-2-carbaldehyde via Knoevenagel condensation to obtain **1A** with an 83 % yield. Next, we synthesized the DASA acceptor **2A** from 2,2-dimethyl-1,3,dioxane,4,6-dione (Meldrum's acid) with a yield of 76 % (**Scheme 5.2**).

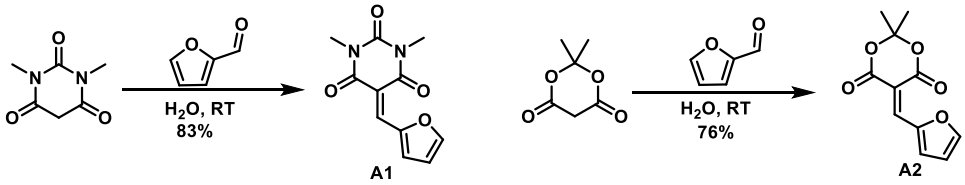

Scheme 5.2 Synthesis of DASA acceptors **A1** and **A2** using 1,3-dimethylbarbituric acid, Meldrum's acid and furan-carbaldehyde via Knoevenagel condensation.

Before the final convergent reaction to synthesize the DASA switch, the donor (**4**) was synthesized. This involved protecting the nitrogen atom in 5-bromoindoline by converting it into tert-butyl carbamate. This was done to guide the coupling of EtO-TEG-OH to the bromine position and prevent any unwanted side reactions that could occur from coupling the nitrogen to the bromine position. To perform the cross-coupling of EtO-TEG-OH to the bromine position of 5-bromoindoline, Buchwald C-O cross-coupling was used where NaO^{t}Bu served as a base and ^{t}BuBrettPhos Pd G3 (**Scheme 5.3**) as a catalyst. The C-O cross-coupling produced product **3** (74 %), which was further re-

acted using TMSI, MeOH, and Et_3N as a base. Deprotection mechanism **3** began with a S_N2 attack of the free electron pair on the TMSI to form **7**, followed by the formation of trimethylsilyl carbamate **8**. Addition of MeOH cleaved the Si-O bond from the trimethylsilyl carbamate, producing methyl trimethylsilyl ether ($MeOSiMe_3$), HI, and carbamic acid **9**, which spontaneously decarboxylated to produce the free amine **4** (**Scheme 5.4**). Finally, the DASA acceptors and donor were condensed in THF with a catalytic amount of water in (aza-)Piancatelli rearrangement reaction.[27–30] The solution changed from colorless/yellowish to deep blue, indicating the formation of the DASA switch (**Scheme 5.5**). The mechanism of the (aza-)Piancatelli reaction (**Scheme 5.6**) elucidates how the condensation reaction between the donor and acceptor part of the DASA occurs and the ring-closing reaction that results in a negative photochromism. Starting from 2-Furylcarbinol (**11**), rearrangement under acidic conditions activates (**i**) for a subsequent nucleophilic attack by the donor part of the DASA, leading to the structure **iii**, corresponding to the open form of the DASA. In the (aza-)Piancatelli reaction, the reaction does not stop at intermediate **iii** but cascades to product **12**, corresponding to the closed form of the DASA switches. Going from **iii** to product **12** occurs via a 4π conrotatory electrocyclization, which resembles the Nazarov cyclization.[10,31]

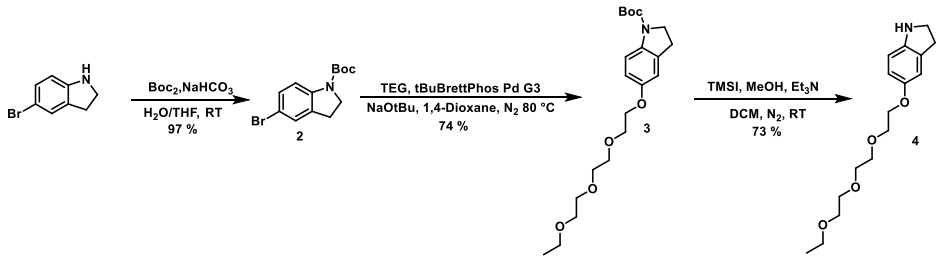

Scheme 5.3 Synthesis of DASA acceptor **4** from 5-bromoindoline via BOC protection **2**, C-O palladium cross coupling **3** and deprotection using TMSI.

The UV-Vis spectra was recorded using 8.3 µM CH_2Cl_2 solution of the respective DASAs: **5** and **6**. We looked into the potential effect of the TEG chain length by comparing Meldrum's acid **6** with methoxyindoline DASA **10**. However, we observed no significant shift in the absorption peaks leading us to conclude the length of the TEG chain does not influence λ_{max}. Both the Meldrum's acids and the 1,3-dimethylbarbituric acid showed absorption maximum λ_{max} at approximately similar wavelength of 600 nm (**Figure 5.1**). The calculation of the open form reveals a delocalization of both the HOMO and LUMO throughout the entire conjugated part. The open and close forms have a difference in energy between their HOMO and LUMO, with the closed form showing a slightly higher band gap of 1.6 eV compared to the 1.34 eV of the open form due to the breaking of the π conjugation.

The transmission probability was calculated using DFT+NEGF. Despite the extended π conjugation resulting in a smaller band gap in the open form compared to the closed form, the transmission probability is lower for the former. This can be explained by Simmon's equation (**Equation 5.1**), where the current density depends on the length d of the

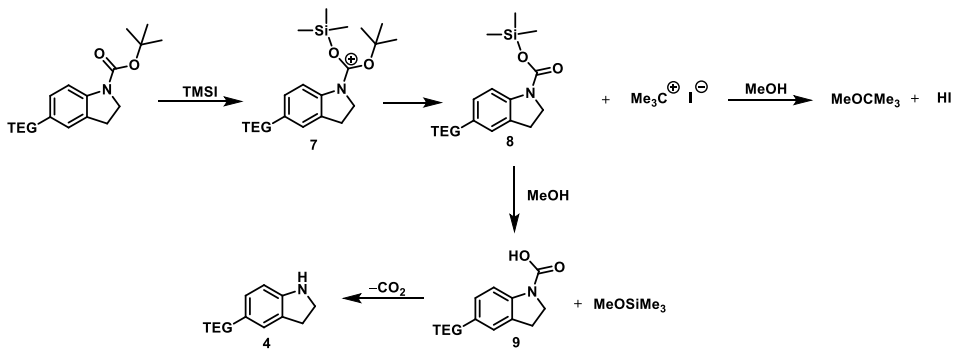

Scheme 5.4 Proposed mechanism of BOC deprotection of DASA donor using TMSI. Formation of TMSI carbamate complex **7**, formation of trimethylsilyl carbamate **8**, cleavage of SI-O bond **9** and subsequent decarboxylation to obtain DASA donor **4**.

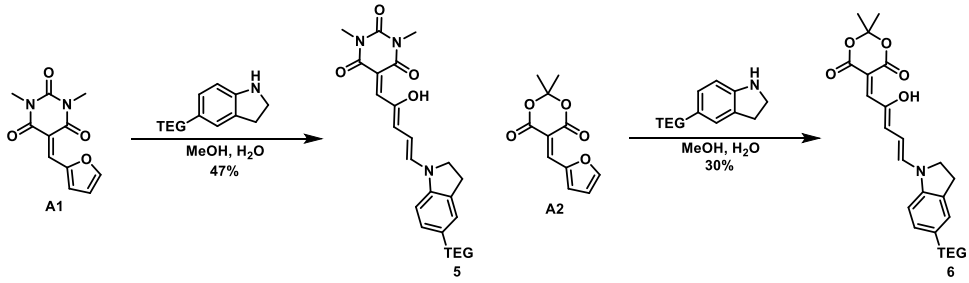

Scheme 5.5 Ring opening of DASA acceptors **A1**, **A2** using DASA donor **4** in a aza-Piacantelli rearrangement fashion to produce TEG-ylated DASA switches **5** and **6**.

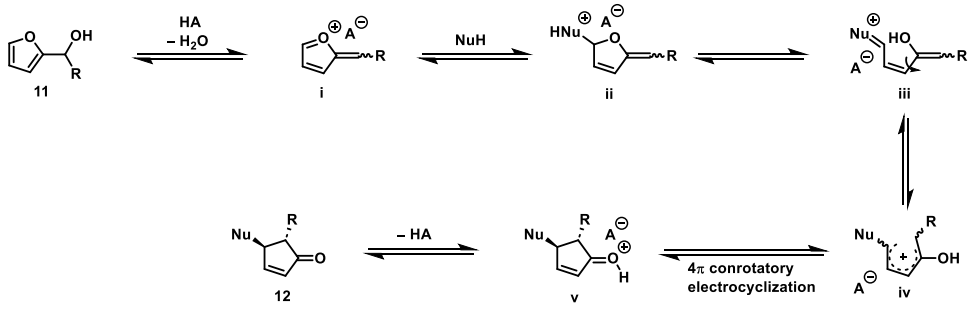

Scheme 5.6 Proposed reaction mechanism of the (aza-)Piancatelli reaction.

molecule. As the open form of DASA **5** is 0.75 nm longer than the closed form (measuring 2.9 nm and 2.15 nm respectively), these results align with the equation.

$$J = J_0 e^{-\beta d} \tag{5.1}$$

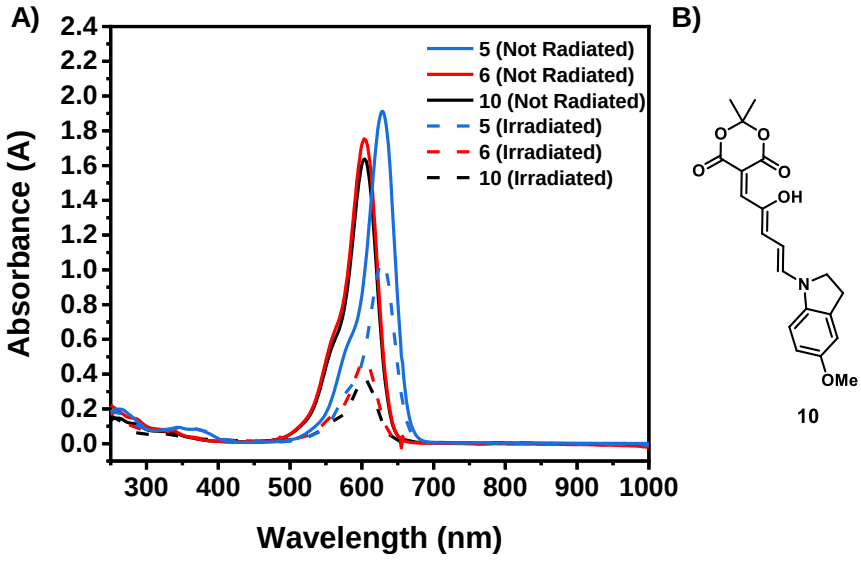

Figure 5.1 UV-Vis of open form of **5**, **6**, and **7** (solid lines), and UV-Vis of **5**, **6**, and **7** after irradiation with 505 nm LED (dashed lines).

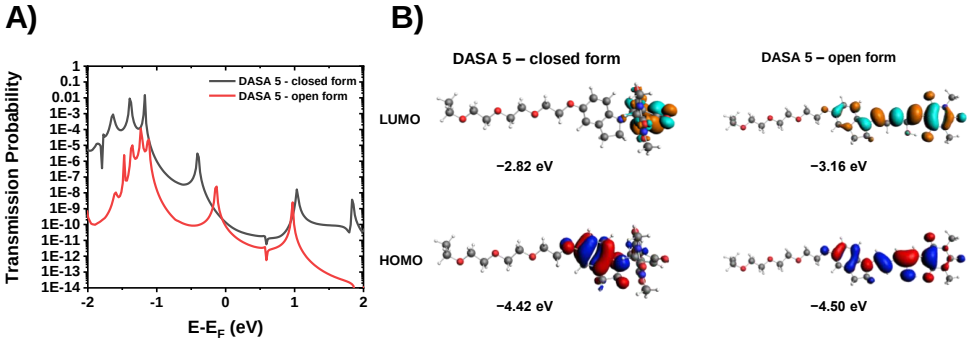

Figure 5.2 A) Transmission calculation probability. B) HOMO-LUMO leves of open and closed form of DASA **5**

5.3. CONCLUSION

We synthesized second generation DASAs by using 1,3-dimethylbarbituric acid (**5**) and Meldrum's acid **6** as acceptors. After comparing the UV-Vis data of DASA (**6**) and the methoxyindoline equivalent of **6**, we found that there was no significant influence of the TEG chain on λ_{max}. We conducted DFT calculations and transport probability using DFT+NEGF on the closed and open form of DASA **5**. We observed that the transmission probability of the open form was lower by an order or two of magnitude, even though its band gap was smaller than the closed one. We attribute these results to the 0.75 nm difference in the length of the molecules.

5.4. EXPERIMENTAL

All reagents were purchased from Sigma-Aldrich, Acros, TCI Europe and used as received unless otherwise stated. Anhydrous THF, DMF were obtained from an in-house Solvent Purification System. For thin layer chromatography (TLC) Merc silica gel 60 F_{254} aluminium plates were used. Visualization of compounds by TLC were done by irradiation with UV light, I_2, $KMnO_4$ or PMA stain. Column chromatography was performed using a Silicagel Kieselgel 60 M(0.04 – 0.063 mm, 230 – 400 mesh). ^{1}H NMR, ^{13}C NMR were performed on Agilent Technologies 400/54 Premium Shielded (400MHz), Varian Oxford AS400 (400MHz) nuclear magnetic resonance spectrometer. The following abbreviations were used to explain NMR peak multiplicities: s = singlet, d = doublet, t = triplet, q = quartet, m = multiplet, br = broad. High resolution mass spectra (HRMS) was recorded on Thermo Scientific LTQ Orbitrap XL (ESI^+, ESI^-, APCI).

5-(furan-2-ylmethylene)-1,3-dimethylpyrimidine-2,4,6(1H,3H,5H)-trione (A1) A 100 mL flask was charged with 1,3-dimethylpyrimidine-2,4,6(1H,3H,5H)-trione (1.56 g, 10 mmol) and 30 mL water followed by dropwise addition of furan-2-carbaldehyde (0.961 g, 10 mmol, 0.83 mL, 1 eq.). The reaction was left stirring for 4 h before filtering and washing it with 2 × 30 mL water. The yellow precipitate was redissolved in CH_2Cl_2, washed sequentially with $NaHSO_3$, H_2O, $NaHCO_3$ and brine. The organic layer was dried over $MgSO_4$, filtered and the solvent was removed under reduced pressure to give the product as bright yellow powder (1.946 g, 83 %).

^{1}H NMR (400 MHz, $CDCl_3$) δ 8.64 (d, J = 3.8 Hz, 1H),8.45 (s, 1H), 7.85 (dd, J = 1.7, 0.7 Hz, 1H), 6.74 (ddd, J = 3.9, 1.7, 0.8 Hz, 1H), 3.41 (d, J = 3.3 Hz, 6H).^{13}C NMR (101 MHz, $CDCl_3$) δ 153.8, 153.0, 143.7, 130.7, 117.8, 79.9, 31.6, 30.9. HRMS - ESI^+ (m/z) Calculated for $C_{11}H_{10}N_2O_4$ $[M+H]^+$: 234.06406 Measured: 321.25498

5-(furan-2-ylmethylene)-2,2-dimethyl-1,3-dioxane-4,6-dione (A2) A 100 mL flask was charged with 2,2-dimethyl-1,3-dioxane-4,6-dione (1 g, 6.9 mmol) and 30 mL water followed by dropwise addition of furan-2-carbaldehyde (0.663 g, 6.9 mmol, 0.57 mL, 1 eq.). The reaction was left stirring for 3 h before filtering it and washing it 2 mL × 30 mL. The yellow precipitate was redissolved in CH_2Cl_2, washed sequentially with $NaHSO_3$, H_2O, $NaHCO_3$ and brine. The organic layer was dried over $MgSO_4$, filtered and the solvent was removed under reduced pressure to give the product as bright yellow powder (1.165 g, 76 %).

^{1}H NMR (400 MHz, $CDCl_3$) δ 8.47 (d, J = 3.8 Hz, 1H), 8.36 (s, 1H), 7.84 (dd, J = 1.7, 0.6 Hz, 1H), 6.75 (ddd, J = 3.9, 1.7, 0.8 Hz, 1H), 1.77 (s, 6H). ^{13}C NMR (101 MHz, $CDCl_3$) δ 165.9, 162.8, 153.0, 152.9, 143.9, 130.7, 117.9, 110.2, 107.2, 30.2. HRMS - ESI^+ (m/z) Calculated for $C_{11}H_{10}N_2O_4$ $[M+H]^+$: 245.04204 Measured: 245.04211

tert-butyl 5-bromoindoline-1-carboxylate (2) A 50 mL flask was charged with 5-bromoindoline (0.5 g, 2.5 mmol), 8 mL THF, 8 mL water, $NaHCO_3$ (0.63 g, 7.5 mmol, 3 eq.) and cooled to 0 °C. After 15 min of stirring, BOC_2O (1.09 g, 5 mmol, 2 eq.) was added, stirred for 30 min, left to warm up to room temperature and left to stir overnight. The reaction mixture was added to water, extracted with EtOAc, dried over $MgSO_4$. The crude mixture was purified using silica chromatography using pentane:EtOAc (90:10 v/v%).

The product was obtained as white powder (0.741 g, quantitative yield).

^{1}H NMR (400 MHz, DMSO-d6) δ 7.58 (s, 1H), 7.37 (q, J = 1.3 Hz, 1H), 7.30 (dd, J = 8.5, 2.1 Hz, 1H), 3.90 (t, J = 8.7 Hz, 2H), 3.06 (t, J = 8.7 Hz, 2H), 1.49 (s, 9H). ^{13}C NMR (101 MHz, DMSO-d6) δ 195.3, 151.0, 132.8, 130.8, 128.9, 116.6, 90.2, 59.8, 50.7, 31.1, 15.0, 10.8, 4.9. HRMS - ESI^{+} (m/z) Calculated for $C_{11}H_{10}N_2O_4$ [M+H]$^{+}$: 245.04204 Measured: 245.04211

tert-butyl 5-(2-(2-(2-ethoxyethoxy)ethoxy)ethoxy)indoline-1-carboxylate (3) A dry Schlenk tube was charged with tert-butyl 5-bromoindoline-1-carboxylate (0.1 g, 0.335 mmol), NaO^{t}Bu (0.0394 g, 0.4 mmol, 1.2 eq.), triethylene glycol monoethyl ether (0.119 g, 0.67 mmol, 0.12 mL, 2 eq.) and 1 mL of anhydrous 1,4-dioxane under inert atmosphere. Following the addition the reaction mixture was sonicated for 5 min before reacting at 80 °C overnight. After cooling down to room temperature, EtOAc was added and the reaction mixture was ran through celite. The organic phase was washed with water, extracted with EtOAc, dried over $MgSO_4$. The solvent was removed under reduced pressure and the crude mixture was purified using silica chromatography using pentane:EtOAc (90:10 v/v %) to obtain the product as yellowish oil (0.4933 g, 74 %).

^{1}H NMR (400 MHz, $CDCl_3$) δ 6.7 (d, J = 2.6 Hz, 1H), 6.6 (dd, J = 8.7, 2.6 Hz, 1H), 4.0 (dd, J = 5.8, 4.0 Hz, 2H), 3.9 (t, J = 8.8 Hz, 2H), 3.8 (dd, J = 5.8, 4.0 Hz, 2H), 3.7 (dd, J = 5.7, 3.2 Hz, 2H), 3.6 – 3.6 (m, 5H), 3.5 (dd, J = 5.6, 3.3 Hz, 3H), 3.5 (q, J = 7.0 Hz, 2H), 3.0 (t, J = 8.6 Hz, 2H), 1.5 (s, 9H), 1.1 (t, J = 7.0 Hz, 3H). ^{13}C NMR (101 MHz, $CDCl_3$) δ 157.10, 117.55, 115.48, 114.67, 75.12, 73.38, 73.28, 73.23, 73.22, 73.20, 73.17, 72.92, 72.40, 72.36, 71.45, 70.61, 69.61, 69.20, 69.16, 64.24, 50.26, 31.07, 17.75. HRMS - ESI^{+} (m/z) Calculated for $C_{21}H_{33}NO_6Na$ [M+Na]$^{+}$: 418.2200 Measured: 418.2193

5-(2-(2-(2-ethoxyethoxy)ethoxy)ethoxy)indoline (4) A dry Schlenk tube was charged with tert-butyl 5-(2-(2-(2-ethoxyethoxy)ethoxy)ethoxy)indoline-1-carboxylate **(3)** (0.493 g, 1.25 mmol), anhydrous CH_2Cl_2 (1.5 mL)and anhydrous TMSI (0.30 g, 1.5 mmol, 0.21 mL, 1.2 eq.) under inert atmosphere. After 40 minutes of stirring 1 mL MeOH was added and the reaction was left to stir for further 40 minutes before adding 1 mL Et_3N. Following 40 minutes of stirring, the solvent was removed under reduced pressure. The crude mixture was purified using silica chromatography using pentane:EtOAc (25:75 v/v %). The product was obtained as yellowish oil (0.2533 g, 73%).

^{1}H NMR (400 MHz, $CDCl_3$) δ 7.77 (d, J = 8.8 Hz, 1H), 7.52 (s, 1H), 6.76 (d, J = 10.9 Hz, 1H), 4.24 (t, J = 8.4 Hz, 2H), 4.05-3.21 (m, 14H), 3.16 (t, 2H), 1.21 (t, J = 7.2 Hz, 3H). ^{13}C NMR (101 MHz, $CDCl_3$) δ 183.9, 179.3, 161.1, 152.3, 138.4, 132.7, 108.5, 99.5, 90.3, 85.2, 68.3, 63.8, 61.3, 49.0, 30.1, 4.09. HRMS - ESI^{+} (m/z) Calculated for $C_{11}H_{10}N_2O_4$ [M+H]$^{+}$: 245.04204 Measured: 245.04211

(E)-5-((2Z,4E)-5-(5-(2-(2-(2-ethoxyethoxy)ethoxy)ethoxy)indolin-1-yl)-2-hydroxypenta-2,4-dien-1-ylidene)-1,3-dimethyldihydropyrimidine-2,4(1H,3H)-dione, (5) A round bottom flask was charged with **A1** (26.5 mg 0.11 mmol), 5-(2-(2-(2-ethoxyethoxy)ethoxy)ethoxy)indoline (33.4 mg, 0.11 mmol), 2 mL of THF and few drops of H_2O and stirred overnight. The following day the reaction mixture was filtered and obtained as dark blue/green solid.

^{1}H NMR (400 MHz), δ 12.32 (d, J = 7.5 Hz, 1H), 7.40 (t, J = 9.9 Hz, 1H), 6.86 – 6.66 (m, 2H), 6.57 (d, J = 9.8 Hz, 2H), 6.49 (t, J = 10.9 Hz, 1H), 5.95 (q, J = 10.9 Hz, 1H), 3.98 (dq, J = 10.5, 5.9 Hz, 4H), 3.80 (t, J = 4.7 Hz, 2H), 3.73 – 3.43 (m, 11H), 3.37 – 3.25 (m, 1H), 3.09 (td, J = 10.1, 5.1 Hz, 8H), 1.16 (td, J = 7.0, 2.6 Hz, 3H). HRMS - ESI$^+$ (m/z) Calculated for $C_{27}H_{34}NO_9$ [M-H]$^+$: 516.22281 Measured: 516.22325

5-((2Z,4E)-5-(5-(2-(2-(2-ethoxyethoxy)ethoxy)ethoxy)indolin-1-yl)-2-hydroxypenta-2,4-dien-1-ylidene)-2,2-dimethyl-1,3-dioxane-4,6-dione, (6) A flask was charged with **A2** (22 mg, 1.1 mmol), 5-(2-(2-(2-ethoxyethoxy)ethoxy)ethoxy)indoline (31.1 mg, 1.1 mmol), 3 mL of THF and few drops of H_2O and stirred overnight. The following day the reaction mixture was filtered to obtain the product as blue solid.

^{1}H NMR (400 MHz, $CDCl_3$ δ 11.39 (s, 1H), 7.64 (d, J = 12.2 Hz, 1H), 7.22 (s, 1H), 7.04 (d, J = 8.5 Hz, 1H), 6.84 (d, J = 8.0 Hz, 2H), 6.72 (d, J = 12.3 Hz, 1H), 6.14 (t, J = 12.2 Hz, 1H), 4.12 (dd, J = 5.7, 4.0 Hz, 4H), 3.86 (dd, J = 5.6, 3.9 Hz, 2H), 3.77 – 3.57 (m, 9H), 3.52 (q, J = 7.0 Hz, 2H), 3.29 (t, J = 8.0 Hz, 2H), 1.80 (d, J = 3.7 Hz, 1H), 1.72 (s, 6H), 1.63 (s, 2H), 1.21 (t, J = 7.0 Hz, 3H). HRMS - ESI$^+$ (m/z) Calculated for $C_{27}H_{34}NO_9$ [M-H]$^+$: 528.23404 Measured: 528.23455

DFT CALCULATION

Density Functional Theory (DFT) calculation[20,21] was performed using the Amsterdam Modeling Suite (AMS)[22] software with GGA-PBE[23] exchange-correlation functional and D3 as dispersion and TZP,[24,25] large frozen core and numerical accuracy using Becke 3 (good)[26] to optimize the open and closed form of DASA 5.

In a paper Verzij *et al.*[32] described an implementation of NEGF formalism for molecular charge transport combined with ADF/BAND periodic band-structure DFT code. We adapted the methodology established by the authors to compute density of states spectra and transmission for metal-molecule-metal junctions.

A geometry optimized molecule is attached to two pyramidal gold tips are constituents of an extended molecule. The extended molecule is attached to a semi-infinite, periodic bulk metal electrode thus creating a well-defined metal-metal interface.

The transport simulations involve four stages. First is the bulk calculation of the electrodes contacts. Second is calculation of the surface's green's function and self-energies. The third step is self-consistent alignment of the potential levels in the electrodes with those in the extended molecule. This yields the E_f of the model system. The final step is the calculation of the transport properties that generates the transmission and DOS spectra.

UV-VIS MEASUREMENTS

UV-Vis was performed on Agilent Cary 8454 UV-Vis Spectrophotometer with a Quantum Northwest temperature controller. The solutions were prepared in CH_2Cl_2 with 8.3 µM concentration.

For studying the closed form and the kinetics of the switching a 15 V, 2.66 A power unit with 3.5 mm jack connector was coupled with a T-cube 1200 mA LED driver and a 505 nm, 8.5 mW, 1000 mA SMA LED from Thorlabs

BIBLIOGRAPHY

[1] F. A. Jerca, V. V. Jerca, R. Hoogenboom, *Nature Reviews Chemistry* **2021**, *6*, 51–69.

[2] X. Jia, L. I. Frye, W. Zhu, S. Gu, T. B. Gunnoe, *Journal of the American Chemical Society* **2020**, *142*, 10534–10543.

[3] A. S. Kozlenko, I. V. Ozhogin, A. D. Pugachev, M. B. Lukyanova, I. M. El-Sewify, B. S. Lukyanov, *Topics in Current Chemistry* **2023**, *381*, DOI 10.1007/s41061-022-00417-2.

[4] M. Irie, T. Fukaminato, K. Matsuda, S. Kobatake, *Chemical Reviews* **2014**, *114*, 12174–12277.

[5] A. Gerwien, T. Reinhardt, P. Mayer, H. Dube, *Organic Letters* **2017**, *20*, 232–235.

[6] D. J. van Dijken, P. Kovaříček, S. P. Ihrig, S. Hecht, *Journal of the American Chemical Society* **2015**, *137*, 14982–14991.

[7] R. Castagna, G. Maleeva, D. Pirovano, C. Matera, P. Gorostiza, *Journal of the American Chemical Society* **2022**, *144*, 15595–15602.

[8] H. Zulfikri, M. A. J. Koenis, M. M. Lerch, M. Di Donato, W. Szymański, C. Filippi, B. L. Feringa, W. J. Buma, *Journal of the American Chemical Society* **2019**, *141*, 7376–7384.

[9] N. Mallo, E. D. Foley, H. Iranmanesh, A. D. W. Kennedy, E. T. Luis, J. Ho, J. B. Harper, J. E. Beves, *Chemical Science* **2018**, *9*, 8242–8252.

[10] M. M. Lerch, M. Di Donato, A. D. Laurent, M. Medved', A. Iagatti, L. Bussotti, A. Lapini, W. J. Buma, P. Foggi, W. Szymański, B. L. Feringa, *Angewandte Chemie International Edition* **2018**, *57*, 8063–8068.

[11] M. M. Lerch, S. J. Wezenberg, W. Szymanski, B. L. Feringa, *Journal of the American Chemical Society* **2016**, *138*, 6344–6347.

[12] J. R. Hemmer, Z. A. Page, K. D. Clark, F. Stricker, N. D. Dolinski, C. J. Hawker, J. Read de Alaniz, *Journal of the American Chemical Society* **2018**, *140*, 10425–10429.

[13] S. Helmy, S. Oh, F. A. Leibfarth, C. J. Hawker, J. Read de Alaniz, *The Journal of Organic Chemistry* **2014**, *79*, 11316–11329.

[14] N. Mallo, P. T. Brown, H. Iranmanesh, T. S. C. MacDonald, M. J. Teusner, J. B. Harper, G. E. Ball, J. E. Beves, *Chemical Communications* **2016**, *52*, 13576–13579.

[15] J. R. Hemmer, S. O. Poelma, N. Treat, Z. A. Page, N. D. Dolinski, Y. J. Diaz, W. Tomlinson, K. D. Clark, J. P. Hooper, C. Hawker, J. Read de Alaniz, *Journal of the American Chemical Society* **2016**, *138*, 13960–13966.

[16] V. A. Barachevsky, *Review Journal of Chemistry* **2017**, *7*, 334–371.

[17] S. Kumar, S. Soni, W. Danowski, I. F. Leach, S. Faraji, B. L. Feringa, P. Rudolf, R. C. Chiechi, *The Journal of Physical Chemistry C* **2019**, *123*, 25908–25914.

[18] S. Kumar, J. T. van Herpt, R. Y. N. Gengler, B. L. Feringa, P. Rudolf, R. C. Chiechi, *Journal of the American Chemical Society* **2016**, *138*, 12519–12526.

[19] X. Qiu, V. Ivasyshyn, L. Qiu, M. Enache, J. Dong, S. Rousseva, G. Portale, M. Stöhr, J. C. Hummelen, R. C. Chiechi, *Nature Materials* **2020**, *19*, 330–337.

[20] P. Hohenberg, W. Kohn, *Phys. Rev.* **1964**, *136*, B864.

[21] W. Kohn, L. J. Sham, *Phys. Rev.* **1965**, *140*, A1133.

[22] Vrije Universiteit, Amsterdam, The Netherlands, *AMS 2022.1, SCM, Theoretical Chemistry*, version 2022.1.

[23] M. Ernzerhof, G. E. Scuseria, *The Journal of chemical physics* **1999**, *110*, 5029–5036.

[24] E. Van Lenthe, E. J. Baerends, *J. Comput. Chem.* **2003**, *24*, 1142–1156.

[25] D. P. Chong, E. Van Lenthe, S. Van Gisbergen, E. J. Baerends, *J. Comput. Chem.* **2004**, *25*, 1030–1036.

[26] M. Franchini, P. H. T. Philipsen, L. Visscher, *J. Comput. Chem.* **2013**, *34*, 1819–1827.

[27] S. Helmy, F. A. Leibfarth, S. Oh, J. E. Poelma, C. J. Hawker, J. R. de Alaniz, *Journal of the American Chemical Society* **2014**, *136*, 8169–8172.

[28] O. N. Faza, C. S. López, R. Álvarez, Á. R. de Lera, *Chemistry - A European Journal* **2004**, *10*, 4324–4333.

[29] C. Piutti, F. Quartieri, *Molecules* **2013**, *18*, 12290–12312.

[30] D. R. Wenz, J. R. de Alaniz, *Organic Letters* **2013**, *15*, 3250–3253.

[31] W. T. Spencer III, T. Vaidya, A. J. Frontier, *European Journal of Organic Chemistry* **2013**, *2013*, 3621–3633.

[32] C. J. O. Verzijl, J. M. Thijssen, *The Journal of Physical Chemistry C* **2012**, *116*, 24393–24412.

LIST OF ACRONYMS

Abbreviation	Decription
2PACz	(2-(9H-carbazol-9-yl)ethyl)phosphonic acid
$4NH_3CzI$	4-aminobutylferrocene hydroiodide
AFM	Atomic Force Microscopy
Ag^{TS}	Template stripped Ag
AMS	Amsterdam Modeling Suit
APCI	Atmospheric-pressure chemical ionization
Au^{TS}	Template stripped Au
BCP	Bathocuproine
β	Tunneling Decay Coefficient
Br-2PACz	(2-(3,6-Dibromo-9H-carbazol-9-yl)ethyl)phosphonic acid
C60	Buckminsterfullerene
CB	Conduction Band
CIGS	Cu, In, Ga, Se solar cell
CnPA	Alkyl phosphonic acid
d	Tunneling barrier length
D3	Damping of third order
DASA	Donor-acceptor Stenhouse adducts
DJ	Dion-Jacobsen
DMF	Dimethylformamide
DMSO	Dimethylsulfoxide
EGaIn	Eutectic Ga In
EQE	External Quantum Efficiency
ESI^-	Electrospray Ionization Negative Ion Mode
ESI^+	Electrospray Ionization Positive Ion Mode
Et_3N	Triethylamine
η	Power Conversion Efficiency
ETL	Electron Transporting Layer
EtOAc	Ethyl Acetate
FA	Formamidinium
FcPA	(4-ferrocenylbutyl)phosphonic acid
FF	Fill Factor
γ_L^D	Dispersive component of liquid surface tension
γ_L^P	Polar component of liquid surface tension
γ_S	Surface free energy of solid
γ_S^D	Dispersive component of surface free energy of solid
γ_S^P	Polar component of surface free energy of solid

GGA-PBE	Generalized Gradient Approximation with Perdew-Burke-Ernzerhof
HOMO	Highest Occupied Molecular Orbital
HTL	Hole Transporting Layer
I_{SC}	Short-circuit current
ITO	Indium Tin Oxide
J_0	Injection Current Density
J-V	Current-Voltage
KPFM	Kelvin Probe Force Microscopy
λ_{MAX}	Wavelength at which a substance has the highest absorption
LED	Light Emitting Diode
LUMO	Lowest Unoccupied Molecular Orbital
MA	Methylammonium
MACl	Methylammonium Chloride
MO	Molecular Orbital
MPP	Maximum Power Point
NEXAFS	Near-edge X-ray Absorption Fine Structure Spectroscopy
NIR	Near Infrared Region
OPV	Organic Photovoltaic
P3HT	Poly(3-Hexylthiophene)
PA	Phosphonic Acid
PCE	Power Conversion Efficiency
PEACl	Phenethylammonium Chloride
PEDOT:PSS	Poly(3,4-ethylenedioxythiophene) polystyrene sulfonate
PLD	Pulsed Laser Deposition
PMA	Phosphomolybdic Acid
P_{MAX}	Maximum Power
PM-IRRAS	Polarization Modulation-Infrared Reflection Absorption Spectroscopy
PTEG-1	Buckminsterfullerene Derivative with triethylene glycol chain
R	Rectification
RF-O_2 plasma	Radio-Frequency O_2 Plasma
RMS	Root Mean Square
RP	Ruddlesden-Popper
SAB	Self-Assembled Bilayer
SAM	Self-Assembled Monolayer
SC3Fc	3-ferrocenylpropylthiol
SEM	Scanning Electron Microscopy
S_N2	Bimolecular Nucleophilic Substitution
SPIRO-OMeTAD	2,2',7,7'-Tetrakis[N,N-di(4-methoxyphenyl)amino]-9,9'-spirobifluorene
TEAI	2-thiophenethylammonium Iodide
TEG	Triethylene glycol
θ	Contact Angle
θ_a	Advancing Contact Angle
θ_r	Receding Contact Angle
THF	Tetrahydrofuran

ThMAI	2-thiopheneethylammonium Iodide
TMSBr	Trimethylsilyl Bromide
TMSI	Trimethylsilyl Iodide
UV	Ultraviolet
Uv-Vis Spectroscopy	Ultraviolet-Visible Spectroscopy
VB	Valance Band
V_{OC}	Open-Circuit Voltage
XPS	X-Ray Photoelectrone Spectroscopy